EFFECT OF ROTATIONAL INERTIA ON BUILDING RESPONSE TO EARTHQUAKES VIA A CLOSED-FORM SOLUTION

Andrés Alonso-Rodríguez[a*] and Kostantinos Daniel Tsavdaridis[b]

Insitute for Risk and Uncertainty, University of Liverpool. Peach Street, Chadwick Building, L69 7ZF, Liverpool, UK

[b] *School of Civil Engineering, Faculty of Engineering and Physical Sciences, University of Leeds, Woodhouse Lane, LS2 9JT, Leeds, UK*

[*]andalon@gmail.com

ABSTRACT

In this paper, a widely used building model, comprised of uniform coupled flexural and shear beams, herein improved by allowing for the effects of rotational inertia. Closed-form solutions in terms of trigonometric and hyperbolic functions are obtained, allowing for the explicit formulation of period ratios, modal participation factors, mode shapes, and mode shape derivatives based solely on displacement response, without coupling with chord rotations, which is the case for the Timoshenko beam model. This makes the model proposed in this study more convenient for assessing building behaviour to ground motion, by explicitly highlighting the effect of rotational inertia in their response to earthquakes, making the case for studying their beneficial effects in mitigating response of buildings to ground motion. It is observed that rotational inertia induces mild fundamental period lengthening, while notably reducing period ratios between higher modes and the fundamental one. This can lead to an enhanced response to ground motion showcasing narrow-band characteristics. However, the most severe effect is found to be on the modal participation factor, which is significantly diminished. This leads to important reductions on the overall response, as a consequence of attenuation of the first-mode response, along with severe undercutting of the effects of higher modes. The results demonstrate that without considering the rotational inertia in the assessment of in-plane structural response to horizontal ground motion can lead to conservative results. Moreover, the results showcase the advantages of providing supplemental rotational inertia as a way to improve the seismic behaviour of buildings.

Keywords: Rotational inertia, closed-form solutions, building earthquake response, drift, and acceleration demands.

1. Introduction

The purpose of this work is to inquire systematically about the role of rotational inertia in modifying building response to ground motion. This is achieved by assessing how period ratios, mode shapes, and mode shape derivatives are influenced by the rotational inertia. For this purpose, a low level, continuous representation of these structures through cantilever beams. This allows for the formulation of closed-form expressions that describe its structural behaviour.

Unlike finite element (FE) model solutions, which allow for efficient computation of response of particular cases, closed-form solutions are well suited for the assessment of large populations of buildings as they establish explicit non-dimensional expressions for describing the structural response, thus providing ways for scaling and formulation of general rules. Consequently, generalized models uncover overall behavioural trends that are common to buildings with similar typological behaviour. Moreover, they usually involve a low number of parameters achieving a high level of synthesis, while proper setup of FE models requires the definition of properties of each structural element, which induces a complexity of at least an order of magnitude larger. Moreover, FEM assessments focus mostly on specific cases, without providing for a straight way to uncover trends that apply to other cases. Consequently, risk assessment of urban areas is carried out considering prototype structural models that artificially cluster building among classes that are characterized by fragility curves (Lallemant et al., 2015) or large building conglomerations which are represented by simplified structural models within large scale computer simulations when extensive resources are available (Xu et al., 2014). Closed-form solutions can supplement the latter approach, by providing a better way to

assess building response considering analytical expressions that can be evaluated efficiently by computers.

One of the fundamental beam theories that include effects of rotational inertia on the response, is the Timoshenko beam. However, its modal response is not unconditionally separable on displacements alone. Therefore, assessments involving it require explicit inclusion of both displacement and neutral axis rotation (Benaroya and Wei., 1999), making its implementation difficult for evaluating solely the effects of rotational inertia on earthquake building response. Moreover, shear and flexural deformations occur sequentially in the Timoshenko beam, meaning that their causal systems are in series. This is not the case of buildings, where frames, which deform to later loads resembling patterns observed in shear beams, are coupled together with structural walls; thus, both are subjected to the same displacements. Therefore, they are functionally arranged in parallel.

This study allows for systematic and direct assessment of the effects of rotational inertia in buildings through a model that involves the Bernoulli beam coupled with a shear beam, in such a way that both are subjected to the same lateral displacements. This model has been successfully employed to perform wide-ranging structural identification of hundredths of buildings (Alimoardi et al., 2006) and has been extended to assess effects of building earthquake responses considering base flexibility (Balendra, 1984; Cruz and Miranda, 2018), non-uniform stiffness along height (Alonso-Rodriguez and Miranda 2016.) and rotational ground motions and inelastic behaviour at the base (Meza-Fajardo, Papageorgiou 2018, 2019). Particularly coupled-beam models are useful for studying soil-structure interaction (Stojanović and Petković 2013 ; Stojanović et al., 2017).

Thus, this paper fills a gap in knowledge regarding the understanding of how rotational inertia affects the seismic response of buildings. Consequently, it provides a

rationale for development and deployment of earthquake protection systems using "artificial" rotational inertia. Artificial rotational inertia is provided by mechanical devices that generate restoring forces proportional to overall rotational acceleration without increasing the structure's mass. Instead, it is achieved by coupling gears and gyroscopes to mimic the effect of distributed large masses. (Hu et al., 2014; He, Xie and Wang, 2017). Results of these study show that rotational inertia can have a sizable effect on reduction seismic response for all modes over the entire length of the building, thus providing a strong framework to advance research and development of these devices.

2. Model Definition

As it is aforementioned, the model considered in this study is comprised of uniform Bernoulli and shear beams joined by rigid links articulated at their ends to ensure their joint displacement without constraining the rotation. The model represents buildings as cantilevers with a fixed base, as shown in Figure 1. It was firstly proposed by Osawa (1965) to represent building behaviour to earthquake-induced ground motion for the establishment of design guidelines. Since its inception, it has been employed with multiple purposes, as presented in the introduction.

This large range of uses is possible due to its inherent flexibility. The Miranda-Osawa model proposes modal solutions for the equation of motion considering solely displacement as a variable; whereas the Timoshenko beam model formulation couples displacements and rotations, requiring joint solution of two differential equations. In this study, the model is improved to account for the effects of rotational stiffness on the response to ground motions.

[Include Figure 1 here]

The assessment of free response will be carried out first. Then the results will be employed to formulate closed-form solutions, ie purely analytical expressions that represent the exact response of the model when subjected to horizontal ground motion; the most representative excitation of buildings due to earthquakes (Kramer, 1996). Figure 2 depicts an equilibrium diagram of a section cut of the model. Shear imbalance along a differential slice induces acceleration on it, according to Newton's second law. (Equation 1)

$$V_{sh} + V_{flx} + \rho \frac{\partial^2 u}{\partial t^2} = 0 \quad (1)$$

[Include Figure 2 here]

Where u is the transverse displacement, V_{sh} is the shear on the shear beam, V_{flx} is the shear on the Bernoulli beam, and ρ is the unitary mass per length of the model. Likewise, moment (M) imbalance in the differential slice induces an additional angular acceleration on it:

$$\frac{\partial M}{\partial Z} - V_{flx} = J \frac{\partial^2}{\partial t^2} \frac{\partial u}{\partial z} \quad (2)$$

Where z is the length coordinate along beam height and J is the rotational inertia per length of the beam ensemble. An explicit relationship between displacement and shear on the shear beam can be formulated if an elastic material is considered, as shown in Equation 3. Likewise, Bernoulli beam theory relates moment and displacement, leading to Equation 4.

$$V_{sh} = -AG \frac{\partial u}{\partial z} \quad (3)$$

$$M = EI \frac{\partial^2 u}{\partial z^2} \quad (4)$$

Where AG is the shear stiffness of the shear beam and EI the flexural stiffness of the Bernoulli beam. After replacing (3) and (4) into (2) and performing some algebraic manipulations, the partial differential equation of motion governing the behaviour of the model can be stated as:

$$EI\frac{\partial^4 u}{\partial z^4} - AG\frac{\partial^2 u}{\partial z^2} - J\frac{\partial^4 u}{\partial z^2 \partial t^2} + \rho\frac{\partial^2 u}{\partial t^2} = 0 \quad (5)$$

Where J is the rotational inertia per unitary length. Equation 5 can be reformulated in non-dimensional form as:

$$\frac{\partial^4 u}{\partial x^4} - \alpha^2\frac{\partial^2 u}{\partial x^2} - {J_r}^2\tau^2\frac{\partial^4 u}{\partial x^2 \partial t^2} + \tau^2\frac{\partial^2 u}{\partial t^2} = 0 \quad (6)$$

Where x is a non-dimensional length coordinate ($x = z/H$). For further details on the fundamental concepts supporting Equations 1, 2, 5 and, 6 the reader is referred to Sae-Long et al., (2020) and Chau-Dinh and Le-Tran, (2020). The following parameters have been introduced in Eq. 6:

$$\alpha^2 = \frac{H^2 AG}{EI}; \qquad \tau^2 = \frac{\rho H^4}{EI}; \qquad Jr^2 = \frac{J}{\rho H^2} \quad (7)$$

Where H is the building height, α is the ratio between flexural and shear stiffness and will define trends on deformation patterns. A low value will indicate that flexural type deformations dominate, which is what is observed in buildings where the lateral-load resistance system is predominantly comprised of walls. On the contrary, a large value (α > 20) is observed in buildings that have deformation patterns that resemble shear beams, as it is normally noticed on framed buildings (Malaga-Chuquitaype et al., 2019).

Equation 6 can be solved through separation of variables, hence it can be reformulated as the following coupled ordinary differential equations:

$$q^{II}(t) + \omega^2 q(t) = 0 \quad (8)$$

$$\phi^{IV}(x) - (\alpha^2 - \omega^2\tau^2 Jr^2)\phi^{II}(x) - \omega^2\tau^2\phi(x) = 0 \quad (9)$$

While Equation 8 governs the behaviour of a Single Degree of Freedom (SDOF) oscillator with circular frequency ω; Equation 9 is the ordinary differential equation that defines the mode shapes, which set spatial trends of response. Its general solution follows the form:

$$\phi(x) = A_1 sin(\gamma x) + A_2 cos(\gamma x) + A_3 sinh(\beta x) + A_4 cosh(\beta x) \quad (10)$$

While γ and β are related to model parameters and ω through the following expressions:

$$\omega^2 \tau^2 = \frac{\alpha^2 + \gamma^2 - \beta^2}{Jr^2} \quad (11)$$

$$\alpha^2 + \gamma^2 - \beta^2(1 + \gamma^2 Jr^2) = 0 \quad (12)$$

3. Mode Shapes

Specific solutions to Equation 10 must account for boundary conditions. In this work, building foundations are considered to be stiff enough to prevent displacements and rotations at the base, leading to fixed supports. Therefore, displacements and rotations are required to be zero for $x = 0$.

$$\phi(x)|_{x=0} = 0 \quad (13)$$

$$\phi'(x)|_{x=0} = 0 \quad (14)$$

Likewise, no point masses or time-dependent external forces are considered above the upper-most level, consequently both moment and total shear must be null at $x = 1$. According to Equation (4), the zero-moment condition will be satisfied if:

$$\phi''(x)|_{x=1} = 0 \quad (15)$$

Total shear can be found by adding shear actions on each beam, according to Equations 2 and 3. After some algebraic manipulations, Equation 16 can be proposed.

$$\frac{\partial^3 u}{\partial x^3} - Jr^2 \tau^2 \frac{\partial}{\partial t^2} \frac{\partial u}{\partial x} - \alpha^2 \frac{\partial u}{\partial x} = V \quad (16)$$

Therefore, the zero-shear condition at the top is enforced as long as equation 17 holds:

$$\phi^{III}(x)|_{x=1} - (\alpha^2 - Jr^2\tau^2\omega^2)\phi^I(x)|_{x=1} = 0 \quad (17)$$

Thus, if Equation 11 is replaced in Equation 17, this boundary condition becomes:

$$\phi^{III}(x)|_{x=1} - (\beta^2 - \gamma^2)\phi^I(x)|_{x=1} = 0 \quad (18)$$

All boundary conditions along with the general solution presented in Equation 10 lead to the following modal characteristic equation, whose roots define a set of particular solutions that satisfy both the partial differential equation of motion and the specific boundary requirements.

$$2\beta^2\gamma^2 + (\beta^4 + \gamma^4)\cosh(\gamma)\cosh(\beta) + \beta\gamma(\beta^2 - \gamma^2)\sin(\gamma)\sinh(\beta) = 0 \quad (19)$$

Equations 19 and 12 define a system of non-linear equations that set values of β and γ. Both equations have an infinite number of discrete roots, that allow for the definition of an infinite number of $\phi(x)$ functions, the mode shapes, which are given by Equation 20. Each one will be associated with a unique circular vibration frequency through Equation 11.

$$\phi_i(x) = sin(\gamma x) - \eta_i cos(\gamma x) - \frac{\gamma_i}{\beta_i} sinh(\beta_i x) + \eta_i cosh(\beta_i x) \quad (20)$$

Where the ϕ i parameter is:

$$\eta_i = \frac{\gamma_i^2 \sin(\gamma) + \gamma\beta \sinh(\beta)}{\beta^2 \cosh(\beta) - \gamma^2 \cosh(\gamma)} \quad (21)$$

Equation 20 is the same one that describes mode shapes in the model without considering rotational inertia (Miranda and Akkar, 2006).

4. Modal Response to Ground Motion

As inertial actions are observed due to both displacement and rotations, Betti's law leads to different mode orthogonality conditions than the ones observed for beams where the effects of rotational inertia are discarded. In specific:

$$\int_0^1 \phi_i(x)\phi_j(x) + Jr^2\phi'_i(x)\phi'_j(x)dx = 0 \quad i \neq j \tag{22}$$

The following supplementary orthogonality conditions can be established:

$$\int_0^1 \phi_i{}^{III}(x)\phi_i^I(x)dx - \alpha^2 \int_0^1 \phi'_i(x)\phi'_j(x)dx = 0 \quad i \neq j \tag{23}$$

$$\frac{j_r^2}{\alpha^2}\int_0^1 \phi_i{}^{III}(x)\phi_i^I(x)dx - \int_0^1 \phi_i(x)\phi_j(x)dx = 0 \quad i \neq j \tag{24}$$

The equation of motion of a beam, when subjected to ground motion, is given by:

$$\frac{\partial^4 u}{\partial x^4} - \alpha^2\frac{\partial^2 u}{\partial x^2} - Jr^2\tau^2\frac{\partial^4 u}{\partial x^2 \partial t^2} + \tau^2\frac{\partial^2 u}{\partial t^2} = -\tau^2\frac{\partial^2 u_g}{\partial t^2} + \tau^2 H\frac{\partial^2 r_g}{\partial t^2} \tag{25}$$

Boundary conditions leading to the orthogonality conditions presented in Equations 23, 24, and, 25 make feasible a solution through modal analysis (Chopra, 2016). In particular, the acceleration response along building height is given by the following expression:

$$\ddot{u}_T(x,t) \approx \sum_{i=1}^N \Gamma_i\phi_i(x)\ddot{\eta}_i(t) + \ddot{u}_g \tag{26}$$

Where u_t is the total displacement from an inertial reference frame, ϕ_i denotes mode shapes according to equation 20, while η_i and Γ_i are given by:

$$\omega_i^2\eta_i(t) + \ddot{\eta}_i(t) = -\ddot{u}_g \tag{27}$$

$$\Gamma_i = \frac{\int_0^1 \phi_i(x)dx}{\int_0^1 \phi_i{}^2(x)dx + J_r\int_0^1[\phi_i{}'(x)]^2 dx} \tag{28}$$

η_i is the response to ground motion of an SDOF with a circular vibration frequency equal to the on mode being considered, while Γ_i is called the modal participation factor and scales each mode contribution to total response. If an infinite number of modes is considered, Equation 26 will provide an exact value of acceleration. However, a reasonable result can be obtained by including as many 6 modes, if the rotational inertia is not considered ($J_r = 0$) (Miranda and Taghavi, 2005).

Similarly, it is possible to estimate the story drift ratio (IDR) defined as the ratio between displacements of successive building levels divided by the story height between

them. Thus, an upper-level estimate can be taken by calculating the derivative of the deflection shape as shown in Equation 29. This parameter highly conditions non-structural and structural damage in buildings (Priestley et al., 2008).

$$IDR(x,t) \approx \sum_{i=1}^{N} \Gamma_i \phi'_i(x) \eta_i(t) \quad (29)$$

Furthermore, it is clear how acceleration demands and drift demands inside buildings are conditioned by mode shapes and their derivatives, respectively. It must be stressed that products $\Gamma_i \phi_i(x)$ and $\Gamma_i \phi'_i(x)$ are unique as long α and J_r parameters are defined, while modal shapes can be arbitrarily scaled.

5. Limit Cases

If $J_r = 0$, the beam deprecates to the Osawa model (1965). For this condition, the γ and β parameters are related by the following expression:

$$\alpha^2 + \gamma^2 - \beta^2 = 0 \quad (30)$$

Which is equivalent to Equation 12 in Miranda and Akkar (2006),

$$2\gamma^2\beta^2 + (2\gamma^2\beta^2 + \alpha^2)\cos(\gamma)\cosh(\beta) + \alpha^2\gamma\beta\sin(\gamma)\sinh(\beta) = 0 \quad (31)$$

After expressing α in terms of β and γ following Equation 30, Equation 31 becomes:

$$2\gamma^2\beta^2 + (\beta^4 + \gamma^4)\cos(\gamma)\cosh(\beta) + \gamma\beta\,(\beta^2 - \gamma^2)\sin(\gamma)\sinh(\beta) = 0 \quad (32)$$

Which demonstrates that the Osawa beam (1965) is a particular case of the proposed model in this study. Similarly, the orthogonality condition becomes:

$$\int_0^1 \phi_i(x)\phi_j(x)dx = 0 \quad i \neq j \quad (33)$$

Similarly, if $\alpha = 0$, the Rayleigh beam is described. Its modal characteristic equation for the fixed base and the free end is given by Equation 19 (Han et al., 1999), while the γ and β parameters are related through the following expression (Han et al., 1999):

$$\frac{1}{\beta^2} - \frac{1}{\gamma^2} = {J_r}^2 \quad (34)$$

After a few algebraic manipulations Equation 34 can be written as:

$$\gamma^2 - \beta^2 = \beta^2 \gamma^2 {J_r}^2 \quad (35)$$

Which is a particular form of Equation 12 when $\alpha = 0$. Likewise, for $\alpha = 0$ the orthogonality condition stated in Equation 23 becomes:

$$\int_0^1 {\phi_i}^{III}(x)\phi_i^I(x)dx = 0 \ \ for\ i \neq j \quad (36)$$

As reported in Han et al. (1999).

6. Effects of rotational inertia on mode shapes

6.1 Effects on period ratios

The fundamental period of vibration suffers a moderate elongation due to the effects of rotational inertia; if the J_r factor is less than 10%, lengthening is less than 5%, independently of the value of α. This is presented in Figure 3, where the fundamental periods have been normalized by values observed for beams where the effects of rotational inertia are ignored ($J_r = 0$). It is observed that fundamental periods increase more in walled buildings ($\alpha > 7$) than in framed and braced structures ($\alpha > 20$). Beyond this threshold effects become more significant; for a value of $J_r = 0.25$, period lengthening ranges between 15% and 7%.

[Insert Figure 3 here]

Equation 11 provides a systematic way to define modal period ratios, presenting how higher mode vibration periods are influenced by the rotational inertia. Based on the definition of the circular vibration frequency it is possible to propose the following expression:

$$\frac{T_1}{T_i} = \sqrt{\frac{{\alpha_i}^2 + {\gamma_i}^2 - {\psi_i}^2}{{\alpha_1}^2 + {\gamma_1}^2 - {\psi_1}^2}} \quad (37)$$

Where T denotes modal periods associated with the i-ith and the 1-st (fundamental) modes. Period ratios for the second and third modes are also presented in Figure 3.

The effects on higher modes are significantly larger and driven by the J_r ratio. For values less than 5% differences are negligible, then an almost linear reduction in period ratios is observed beyond this limit. For a beam with J_r = 0.3, period ratios are slightly larger than 0.6 between the fundamental and the second and 0.4 between the fundamental and the third, taking a beam with J_r = 0 as the baseline. For these thresholds, second and third modal periods are more than 50% and twice the values computed when rotational inertia effects are discarded. Differences between beams with $\alpha = 0$ and $\alpha = 20$ are within 5 to 10% making effects of this parameter secondary. Framed buildings (α = 20) experience slightly enhanced period elongation (<10%) than walled buildings ($\alpha = 0$).

6.2 Effects on modal participation factors (MPFs)

Although mode shapes can be arbitrary scaled by setting custom values for any of the coefficients in Equation 10, the product of modal participation factor and mode shape ordinates $\Gamma_i\phi_i(x)$ is unique, as is the result of a particular solution of the partial differential equation of motion governing the behaviour of the model. Consequently, it is possible to systematically assess the effects of ground motion by plotting the ordinates of this product at the top of the building.

[Insert Figure 4 here]

Rotational inertia diminishes MPF values sizably, potentially reducing both acceleration and drift demands in buildings; particularly high-mode response. Moreover, reductions can be sizable beyond J_r = 10%. For this threshold, third- and second-

ordinates are less than one-sixth and one-third respectively of what would be observed in models where rotational inertia is not considered (i.e., $J_r = 0$), as shown in Figure 4. Therefore, providing supplemental rotational inertia could be a cost-effective structural control measure for improving the seismic performance of buildings.

The effects are more prevalent in buildings where the lateral load resistant systems are comprised mostly of walls ($\alpha > 7$) while buildings with frames as their main lateral load support system ($\alpha > 20$) demonstrate lesser reductions. The difference between both cases ranges less than 10%, making the effect of α secondary when compared to the role of J_r.

6.3 Effects on mode shapes

The assessment of first-mode shapes demonstrates that the most critical effect of the rotational stiffness in earthquake response of buildings is the reduction of the MPF factor. For values of $J_r < 0.1$ and $\alpha < 10$ a uniform reduction of modal ordinates is observed; grossly up to 40% for $J_r = 0.3$; following trends described in Figure 4. However, beyond these limits a slight change in the behaviour is observed; modal ordinates show a larger reduction (up to 10%) in the first two-thirds of the beam when compared to peak values at the top (Figure 5).

[Insert Figure 5 Here]

Overall reductions along the height for higher models are more significant; up to 90% for $J_r = 0.3$ and $\alpha = 0$; even for $J_r = 0.05$, modal ordinates are roughly one-third of what is observed for the model without involving rotational inertia. Yet, the maximum response is observed always at the top of the beam ($x = 1.0$). The locations of nodes

(where the mode shape is zero) showcase larger variations for buildings where walls are predominant ($\alpha > 7$). In particular, for $\alpha > 0$ the node is located at $x = 0.78$ for $J_r = 0$, while it migrates to 0.88 for $Jr = 0.3$. The effects are comparable for buildings with frames, as for $\alpha = 0$ the second mode node is at $x = 0.36$, while it migrates to $x = 0.39$ in both cases leading to a difference slightly larger than 11%. Similar trends are observed for anti-nodes (locations where modal ordinates reach a peak value except at the top, $x = 1$).

Regarding the third mode, similar trends are observed; for $J_r = 0.05$, values are in overall terms one-fourth of what is observed for $J_r = 0$ for both walled ($\alpha < 7$) and framed ($\alpha < 20$) buildings, indicating how the effects of mode ordinate attenuation are more significant for higher modes. Node and antinode locations migrate 10% upwards for all α values, as J_r decreases from 0 to 0.3, in an analogous manner to what was described for the second mode.

6.4 Effects on mode shape derivatives

The effects on mode shape derivatives, which condition building drift response, follow trends similar to the ones outlined for mode shapes; albeit mode ordinate attenuation is in overall terms 10% lower, according to Figure 6. Results show that the major feature induced by increasing the rotational inertia is leading to a proportional decrease on the derivatives of mode shapes all over the building height. Changes to their behaviour along height are secondary. This indicates that the major consequence of increasing the rotational inertia is the reduction of the modal participation factor, rather than allowing for significant changes on the γ and β parameters. Thus, it should be expected that drift and acceleration demands are not reduced at particular locations, rather they decrease on all floors.

Regarding peak derivative values for both third and second modes, for the flexural beam (α = 0) maximum values are observed at the top ($x = 1.0$). The positions of the second and third peaks remain practically unchanged as long as $J_r < 0.10$. Then it drifts 10% for $J_r = 0.3$. For the case of $\alpha = 5$, the location of the largest peak value experiences significant variations; as J_r reduces, it tends to be observed closer to the top of the beam, mimicking what is observed in the Bernoulli beam. Eventually when $J_r = 0.3$ it is observed at $x = 0.99$. Second and third peaks, close to the base of the beam, diverge at most 10%, following what is observed for the case α = 0, For buildings where their lateral load resistant system is comprised by frames ($\alpha = 20$) peaks diverge 10% when comparing the locations for beams with $J_r = 0.3$ and $J_r = 0$.

[Insert Figure 6 here]

7. Discussion

The model developed in this study shows that rotational inertia could mitigate the effects of horizontal ground motion in buildings, mainly by reducing the modal participation factor of all modes. Therefore effects can be observed over the entire building height.

Albeit the approach proposed in this study could explain phenomena observed during strong motion, its application into retrofitting of existing structures is, at first sight limited. One option would be to change the mass distribution on the floor plan, to spread it away from the mass centre. However, this option has several downsides, as this could lead to a more significant effect of vertical ground motion, and a potential need to reinforce flooring systems to carry the additional structural demands induced by this course of action. This could render its potential benefits slight.

However, recent work in structural engineering is focusing on mechanical devices that are capable of modifying the earthquake response of buildings, without inducing

residual deformations. One option is the use of supplemental rotational inertia (e.g., Makris, Kampas, 2016) which uses arrangements of gears and flywheels to produce a restoring force that is proportional to the difference of acceleration between its ends; effectively recreating an "equivalent" mass without substantially increasing the structure weight. However, direct attachment of these devices to the structure is not optimal as the difference between accelerations of their extremes under such consideration is at best moderate, consequently, they are coupled with tuned mass dampers to become more efficient (Giaralis andTaflanidis, 2015, Thiers-Moggia and Malaga-Chuquitaype, 2018).

An improvement could be made by providing equivalent rotational inertia instead, through the deployment of vibration control systems based on devices that generate restoring forces directly related to angular momentum, and thus take advantage of the effects found in this study. One promising option is the use of gyroscopes for adaptative behaviour of structures when subjected to dynamic actions, among them earthquakes. (Hu et al., 2014; He, Xie and Wang, 2017).

The approach proposed in this study is intended for assessing the elastic and close-to-elastic response of buildings as it leads to a closed-form solution. Its purpose is studying the behaviour or large stocks of buildings and understanding fundamental phenomena that underpin building response to earthquakes. Particularly it is well-suited for earthquake risk assessments, as the threshold of structural damage is several times larger than the limits at which non-structural damage happens (Charleson 2007, Magenes et al., 2009), thus the later will drive economical losses.

8. Conclusions

A widely applied model for representing large building portfolios within urban areas has been expanded in this study to include the effects of rotational inertia on their structural response when subjected to ground horizontal motion. Modal properties including mode

shapes and mode shape derivatives, which are useful for assessing drift demands within buildings, were obtained in closed-form. Mode shapes are described by a linear combination of four terms; two trigonometric and two hyperbolic functions. The most general mode shape has a similar formulation that resembles previous models that do not include the effects of rotational inertia. Differences are rather observed in how parameters describing mode shapes interact with each other and on the way they come together to define the modal vibration periods.

The most critical effect of rotational inertia is observed on the definition of the Modal Participation Factor for assessing response to horizontal ground motion. It includes an additional term that involves the derivatives of mode shapes, leading to significant reductions on all modes, more significantly on higher ones. Effects can be sizable leading to a diminishing of more than 50% of the second and third modes, even just by providing moderate increases of rotational inertia. Moreover, both acceleration and drift responses are mitigated all over the building height. This effect is specific to the consequences of the horizontal ground motion.

Also, it was observed that there is a mild lengthening of modal periods, reaching at most 10% for the fundamental mode and more than twice for modes beyond the second. At first sight, this could be judged to be moderate; but for ground motion showcasing narrow brand patterns acceleration drift demands could increase notably. Results show that providing supplemental rotational inertia could lead to relevant improvements of earthquake response of buildings, even for moderate seismicity, making a case for further studies on seismic protection strategies which can take advantage of this feature.

9. Acknowledgements

The authors are grateful for the feedback provided by Dr Agatholikis Giaralis from City, University of London, Dr Olga Mavrlouli from the University of Twente and two

anonymous reviewers. Their comments improved greatly the quality of this manuscript.

10. References

Alimoardi A., Miranda E Taghavi S., Naeim F. 2006. Evolutionary modal identification utilizing coupled shear-flexural response - implications for multistory buildings part I theory. The structural design of tall and special buildings 15 : 51-65.

Alonso-Rodriguez A., Miranda E. 2016. Dynamic behavior of buildings with non-uniform stiffness along their height assessed through coupled flexural and shear beams. Bulletin of Earthquake Engineering 14 (2) : 3463-3483.

Alonso-Rodriguez A,. Nikitas N., Knappett J., Kampas G., Anastasopoulos I., Fuentes R. 2018. System identification of tunnel response to ground motion considering a simplified model. Frontiers in Built Environment 2018; 4 (39) 1:11.

Balendra T. 1984. Free vibration of a shear wall-frame building on an elastic foundation. Journal of sound and vibration 96 (4): 437-446.

Charleson A.,2007. Architectural Design for Earthquake: A Guide to the Design of Non-Structural Elements. New Zealand Society for Earthquake Engineering, Wellington, New Zealand.

Chau-Dinh T., Le-Tran N. 2020 An 8-Node Solid-Shell Finite Element based on Assumed Bending Strains and Cell-Based Smoothed Membrane Strains for Static Analysis of Plates and Shells. Journal of Applied and Computational Mechanics; 6 (SI) : 1335-1347.

Chopra A. 2016. Dynamics of structures. 5th ed. Pearson: London, UK

Cruz, C., Miranda E. 2017. Evaluation of soil-structure interaction effects on the damping ratios of buildings subjected to earthquakes. Soil dynamics and Earthquake Engineering 100: 183-195.

Giaralis A., Taflanidis A. 2015. Reliability-based design of tuned mass-dampers-inerter (TMDI) equipped multistorey frame buildings under seismic excitation. Proc., 12th Int. Conf. on Applications of Statistics and Probability in Civil Engineering, ed T. Haukaas.; Vancouver, BC, Canada.

Han S., Benaroya H., Wei T. 1999. Dynamic of transversely vibrating beams using for engineering theories. Journal of sound and vibration 225 (5): 935-988.

He H., Xie X., Wang W. 2017. Vibration control of tower structure with multiple cardan gyroscopes. Shock and Vibration : 3548360.

Hu, Q., Jia Y., Xu S. 2014. Dynamics and vibration suppresion of space structures with control moment gyroscopes. Acta Astronautica 96 : 232-245.

Lallemant D., Kiremidjan A., Burton H. 2015. Statical procedures for producing damage fragility curves. Earthquake Engineering and Structural Dynamics 44 (9): 1373-1389.

Magenes, G., Modena, C., Da Porto, F., and Morandi, P. 2009. Behavior and design of new masonry buildings: Recent developments and consequent effects of design codes, Eurocode 8. Perspectives from the Italian Perspectives Workshop. Doppiavoice, Napoli, Italy : 199-212.

Malaga-Chuquitaype C., Psaltakis M., Kampas G., Wu J. 2019. Dimensionless fragility analysis of seismic acceleration demands through low-order building models. Bulletin of earthquake engineering; Doi: 10.1007/s10518-019-00615-2.

Makris N., Kampas G. 2016. Seismic Protection of Structures with Supplemental Rotational Inertia. Journal of Engineering Mechanics 142 (11): 1-11.

Meza-Fajardo K., Papageorgiou A. 2018. Response of tall buildings to base rocking induced by Rayleigh waves. Earthquake Engineering & Structural Dynamics 47 (8) : 1755 – 1773.

Miranda E. 1999. Approximate seismic lateral deformation demands in multistory buildings. Journal of structural engineering 125 (4): 417 – 425.

Miranda E., Taghavi S. 2005. Approximate floor acceleration demands in multistory buildings. I: formulation. Journal of structural engineering 131 (2): 203-211.

Miranda E., S. Akkar. 2006. Generalized interstory drift spectrum. Journal of structural engineering 132 (6): 840 – 852.

Osawa Y. 1965. Response analysis of tall buildings to strong earthquake motions. Part1: linear response of core-wall buildings. Bull Earthq Res Inst Univ Tokyo 1965; 43:803–817.

Priestley MJN., Calvi GM., Kowalski MJ. 2018. Displacement-based seismic design of structures. 2nd Ed. IUSS Press: Pavia, Italy.

Sae-Long W., Limkatanyu S., Panedpojaman P., Prachasaree W., Damrongwiriyanupap N., Kwon M., Hansapinyo C. (2020) Nonlinear Winkler-based Frame Element with Inclusion of Shear-Flexure Interaction Effect for Analysis of Non-Ductile RC Members on Foundation. Journal of Applied and Computational Mechanics. 6 (SI) : 1572-1580.

Stojanovic V., Kozic P., Petkovic. 2017. Dynamic instability and critical velocity of a mass moving uniformly along a stabilized infinity beam. International Journal of Solids and Structures; 108 : 164-174.

Stojanovic V., Petkovic. 2013. Moment Lyapunov Exponents and Stochastic Stability of a Three-Dimensional System on Elastic Foundation Using a Perturbation Approach. Journal of applied mechanics ASME; 80 (5) :

Thiers Moggia R., Malaga Chuquitaype C. 2018. Seismic protection of rocking structures with inerters. Earthquake Engineering & Structural Dynamics 48 (5) : 528-547.

Xu Z., Lu X., Guan H., Han B., Ren A. 2014. Seismic damage simulation in urban areas based on a high-fidelity structural model and physics engine. Natural Hazards 71:1673-1693.

Figures:

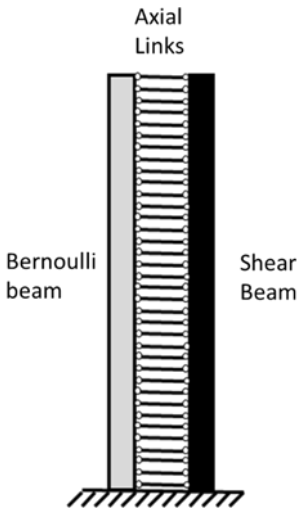

Figure1: Simplified model building. (Miranda 1999)

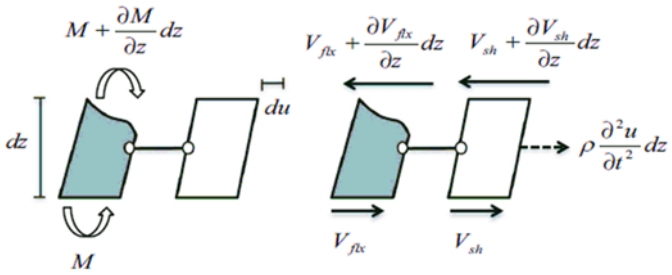

Figure 2: Internal actions in a section cut of the coupled flexural-shear beam. [9]

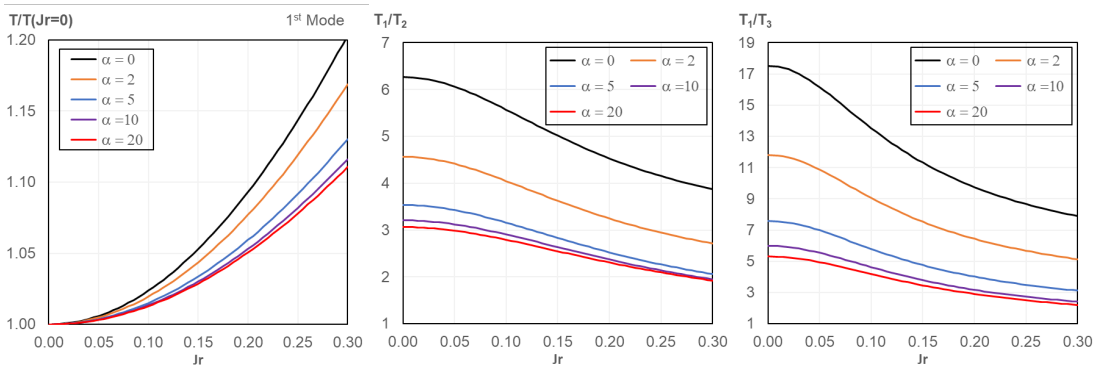

Figure 3: Modal period lengthening with increasing rotational inertia.

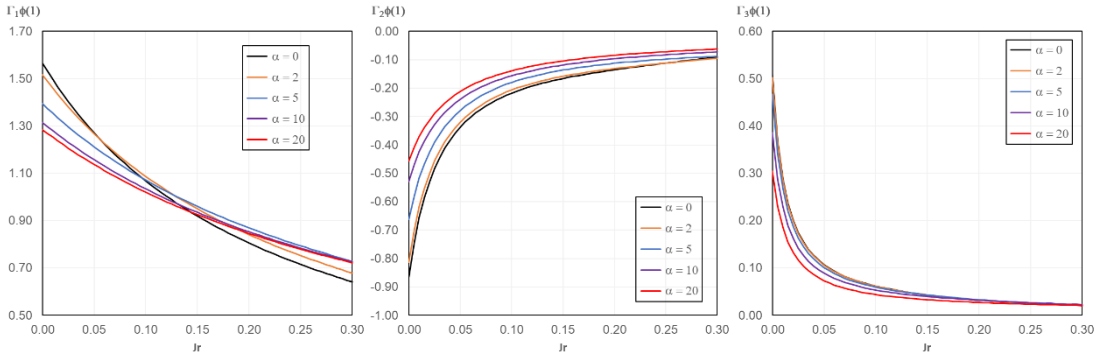

Figure 4: Changes in the MPF normalized modal ordinates with increasing rotational inertia.

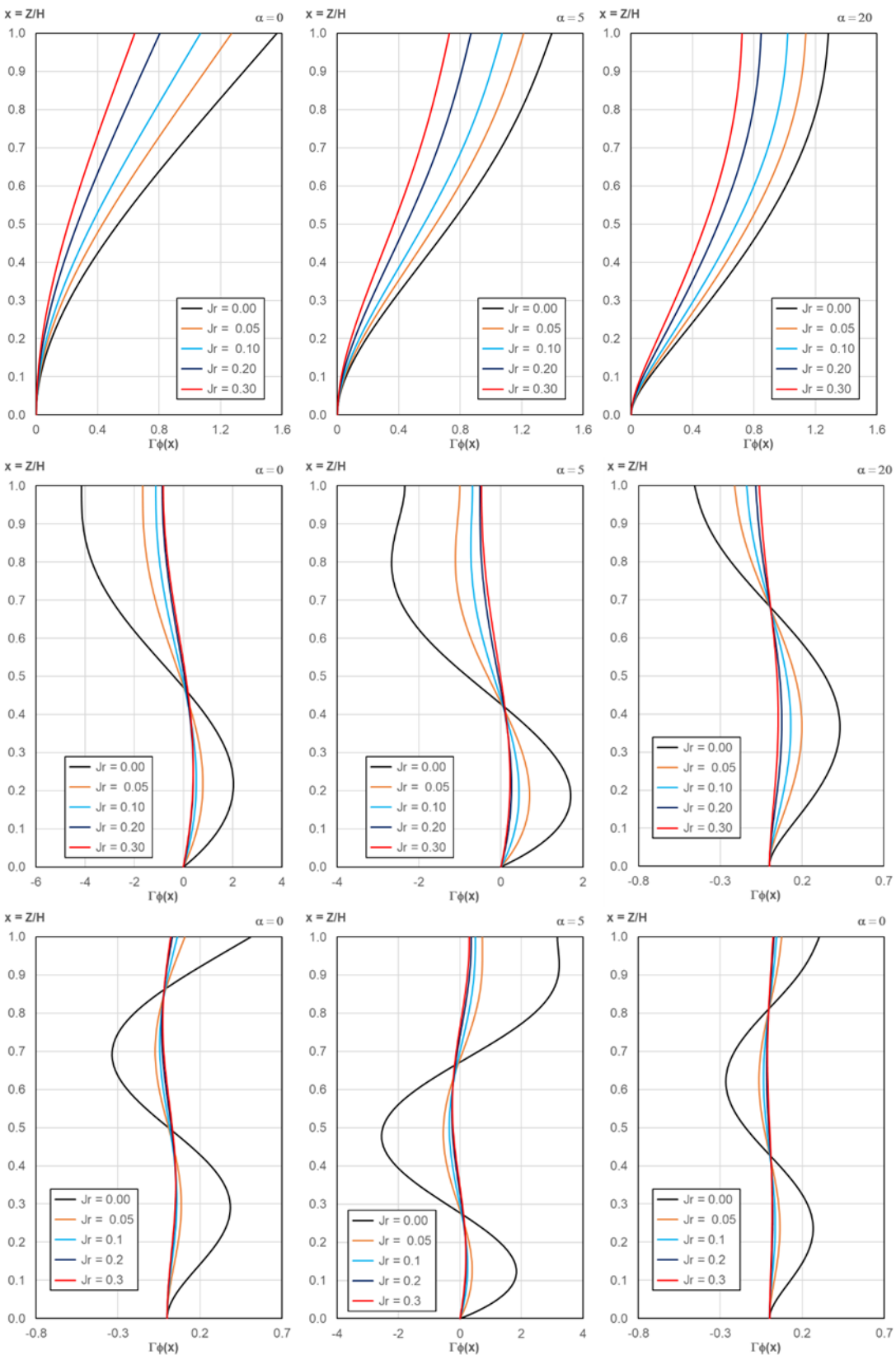

Figure 5: Effects on Modal Ordinates (First Three modes)

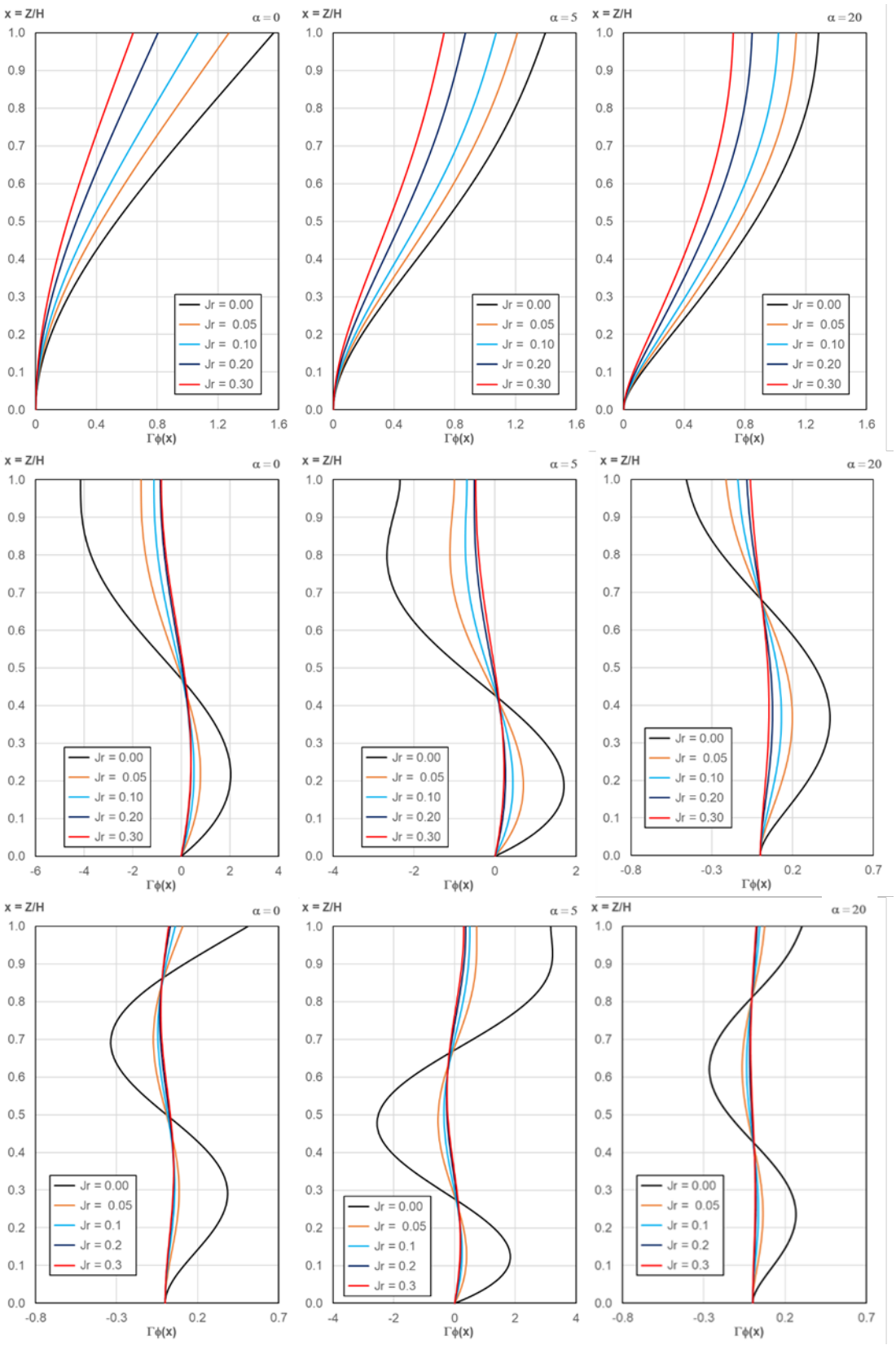

Figure 6: Effects on derivatives of Modal Ordinates (First Three modes)